Second Virial Coefficient of CH$_4$ Vapor in 5 mK–10000 K Temperature Range in Quantum and Classical Regimes

O.T. Al-Obeidat

Department of Physics and Basic Sciences, Faculty of Engineering Technology,
Al-Balqa Applied University, Amman, Jordan

The aim of this work is to study the second virial coefficient B of methane (CH$_4$) vapor over a wide temperature range, $T = 5$ mK–10000 K. The coefficient is calculated in two temperature regions. First, for $T = 5$ mK–20 K — the quantum second virial coefficient B_q is determined for the first time. It is found that the behavior of B_q is similar to that of the CH$_4$–CH$_4$ potential. Standard expressions are then used in this quantum regime at the number density $n = 1 \times 10^{-4}$ Å^{-3} to compute other thermodynamic properties of the system, i.e., the Helmholtz free energy per molecule, the internal energy per molecule, the entropy per molecule and the specific heat capacity. Second, for $T = 20$–10000 K — the classical second virial coefficient B_{cl}, the Boyle temperature T_B and the inversion temperature T_i are determined. The first quantum correction B_{qc} is calculated over the temperature range $T = 20$–100 K. It turns out that it is necessary to make such a quantum correction to B_{cl} for $T = 20$–60 K, whereas the quantum effects are relatively insignificant for $T > 60$ K. In general, our results are in very good agreement with previous theoretical and experimental results.

topics: methane (CH$_4$) vapor, second virial coefficient, quantum corrections, quantum regime

1. Introduction

The second virial coefficient B of a real gas describes the first-order correction to the equation of state of the ideal gas [1] and it can be positive or negative. Positive values indicate overall repulsive interactions, whereas negative values indicate attractive interactions. The second virial coefficient B provides a physical link between the particle interactions (microscopic properties) and thermodynamic (macroscopic) properties of the gas [2]. Further, B can be used to predict the critical point of a liquid–gas transition [3].

In this paper we present calculations of B for CH$_4$ vapor in the broad T-range 5 mK–10000 K. For "low" T (to be defined below), B should behave quantum-mechanically, whereas for higher T, B should behave classically [4–6]. The quantum coefficient B_q is studied starting with the Lippmann–Schwinger (LS) equation [7], which is essentially the Schrödinger equation in momentum space. The LS equation is solved by matrix inversion to give the corresponding phase shifts, which are then fed into the Beth–Uhlenbeck equation to evaluate B_q. On the other hand, both the classical second virial coefficient, B_{cl}, and its first quantum-mechanical correction, B_{qc}, are calculated from standard expressions [8, 9], based only on the intermolecular potential.

The main contribution of the present work, then, is the calculation, for the first time, of B for CH$_4$ down to relatively low T (5 mK), where no experimental data are available. In fact, to the best of our knowledge, no experimental values of high accuracy exist for methane below 150 K. The point is that, at "low" T, quantum effects are expected to make a significant contribution to B. Therefore, B can be used to explore the interface between the classical and quantum regimes in the gas [10–12]. Also, B_q can be considered as an indicator of the formation of small clusters [13]. Novoa and Whangbo [14] found that the methane dimer (CH$_4$)$_2$ is bound in all possible orientations of the molecule.

The abundance of CH$_4$ gas in nature exceeds 90% [15]. It is the simplest representative of the alkanes. A colorless and odorless gas, it is lighter than air. Its melting point is 90.7 K, and its boiling point is 111.65 K [16]. In addition to its increasingly crucial role in modern energetics, it is important for generating electricity when burnt in a steam generator or gas turbine, and it is used in low-temperature fuel cells [16].

For CH$_4$ vapor, B has been the subject of several theoretical [17–24] and experimental [25–29] studies. In general, these have followed closely the same method of computation as for inert gases via the classical cluster expansion, with the Lennard-Jones

potential [22]. A new approach for the exp-6 potential was proposed [30] and the formula was used to calculate B for CH_4 over a broad T-range [30]. Recently, a method for the inverse problem has been reported, namely, obtaining relatively simple intermolecular potentials from (experimental) B [31].

This paper is organized as follows: Sect. 2 is a brief account of the formalism involved, Sect. 3 contains our results and their analysis. Finally, a short conclusion closes the paper in Sect. 4.

2. Formalism

2.1. Quantum second virial coefficient B_q

A full quantum mechanical study is performed to compute B_q over a temperature range 5 mK–20 K. The calculation of B_q is done by determining the phase shifts within the framework of the scattering theory [7]. Then, the calculated phase shifts are inserted into the Beth–Uhlenbeck formula to compute B_q [4].

At low T, B_q is calculated using the Beth–Uhlenbeck formula [4–6]. This is given by

$$B_q(T) = B_{ideal} + B_{bound} + B_{phase}. \tag{1}$$

Here, B_{ideal} is the ideal-gas term, which is important in the low-temperature region, but goes to zero with increasing temperature. Namely,

$$B_{ideal} = -\frac{\lambda^3}{2^{5/2}} = -\frac{1}{2^{5/2}}\left(\frac{2\pi\hbar^2}{mk_BT}\right)^{3/2} \tag{2}$$

where λ is the thermal de Broglie wavelength, m being the CH_4 mass, k_B — the Boltzmann constant and $\hbar = h/2\pi$ (h is Planck's constant).

The bound-state contribution B_{bound} is given by

$$B_{bound} = -2^{3/2}\lambda^3 \sum_{E_B}\left(e^{-\beta E_B} - 1\right). \tag{3}$$

This term is very small and can be neglected [32].

The last term, B_{phase}, represents the contribution of the scattering-state continuum and is given by

$$B_{phase} = -\frac{2^{3/2}\lambda^5}{\pi^2}$$
$$\times \int_0^\infty dk\, k \sum_{\ell=even}(2\ell+1)\,\delta_\ell(k)\,e^{-\beta E(k)}, \tag{4}$$

where $\delta_\ell(k)$ is the ℓ-partial phase shift which is a function of the wave number k. The expression for B_{phase} is obtained as follows [33–35]:

- $V_\ell(k,k')$, which is the Fourier–Bessel transform of $V(r)$ and is needed in the next step, is calculated; k and k' are the incoming and outgoing relative momenta.
- The LS integral equation is solved, using a well-tested matrix-inversion technique, to evaluate $\delta_\ell(k)$. The full technical details are given in [7]. This equation is valid for the present low-dense gas.
- By inserting the values of $\delta_\ell(k)$ in (4), B_{phase} is finally determined.

2.2. Classical second virial coefficient B_{cl}

B_{cl} and its first quantum correction, B_{qc}, are defined by [8, 9]:

$$B_{cl}(T) = 2\pi \int_0^\infty dr\left(1 - e^{-\beta V(r)}\right)r^2, \tag{5}$$

$$B_{qc}(T) = \frac{\pi\hbar^2\beta^3}{6m}\int_0^\infty dr\, e^{-\beta V(r)}\left(V'(r)r\right)^2. \tag{6}$$

Here, $V'(r)$ is the first derivative of $V(r)$ with respect to the magnitude of the intermolecular separation r. The temperature parameter is defined as $\beta = 1/(k_BT)$, and $e^{-\beta V(r)}$ is the classical pair correlation function [36]. Note that B_{qc} is important in the "low"-T regime.

In this study, the "natural" system of units is adopted, i.e., $\hbar = m = k_B = 1$. The conversion factor $\frac{\hbar^2}{m}$ for CH_4 is 3.02386638 K Å².

2.3. CH₄–CH₄ potential

This is our main input, the assumption being that CH_4 molecules are rigid and spherical. The pseudospherical nature of methane suggests that this approximation is not unreasonable [37]. Thus, the methane interaction has been modeled as isotropic [37]; specifically, it is described by the Morse potential [38]:

$$V(r) = D\left(e^{-2\alpha(r-r_e)} - 2e^{-\alpha(r-r_e)}\right), \tag{7}$$

where $D = 149.1$ K, $\alpha = 1.166$ Å^{-1} and $r_e = 4.50$ Å. This is shown in Fig. 1.

3. Results and discussion

3.1. Quantum second virial coefficient B_q

At low enough T, λ becomes comparable to the mean intermolecular distance $\langle r \rangle$. This means that quantum-mechanical effects will dominate and the classical framework will no longer be valid. Now, B_q has its role to play.
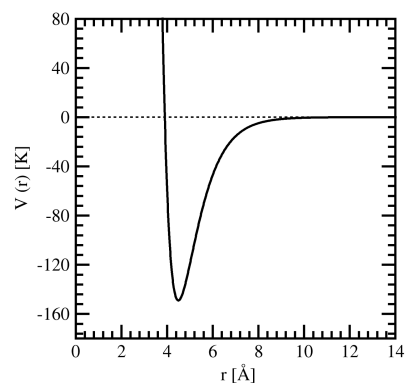
Fig. 1. The CH_4–CH_4 potential $V(r)$ [K] as a function of the intermolecular separation r [Å].

<div style="display:flex">
<div>

TABLE I

The quantum second virial coefficient B_q [cm^3/mol] at different temperatures T [K]. For each T, the ratio of the two terms B_{phase} (5) and B_{ideal} (3) is given.

T [K]	B_q [cm^3/mol]	B_{phase}/B_{ideal}
5×10^{-3}	1.632×10^4	1.66
0.01	1.220×10^4	2.38
0.02	7.582×10^3	3.43
0.03	5.087×10^3	4.00
0.04	3.617×10^3	4.28
0.05	2.754×10^3	4.49
0.1	1.497×10^3	6.37
0.2	1.032×10^3	11.5
0.3	7.900×10^2	15.7
0.4	6.242×10^2	18.9
0.5	4.957×10^2	20.9
1	1.281×10^2	15.5
2	-51.94	15.7
3	-57.88	33.1
4	-43.57	38.5
5	-31.07	38.4
10	-7.022	24.2
15	-2.003	12.2
20	-3.481×10^{-1}	2.53

The results for B_q are given in Table I and in Fig. 2 for $T = 5$ mK–20 K. The density is kept low enough for the system to remain in the vapor phase. Also given in Table I is the ratio of the two terms B_{phase}, given by (5), and B_{ideal}, given by (3). This ratio indicates that B_{phase} dominates for all $T = 5$ mK–20 K.

The behavior of B_q (see Fig. 2) is similar to that of the CH$_4$–CH$_4$ potential (see Fig. 1). The value of B_q is positive for $T < 1.45$ K. This means that the binary interaction is repulsive in this T-regime. By increasing T, B_q decreases. At a particular T, B_q passes through zero at the so-called "unusual" Boyle temperature ($T_B \approx 1.45$ K) [12], and then becomes negative. With increasing T, B_q becomes
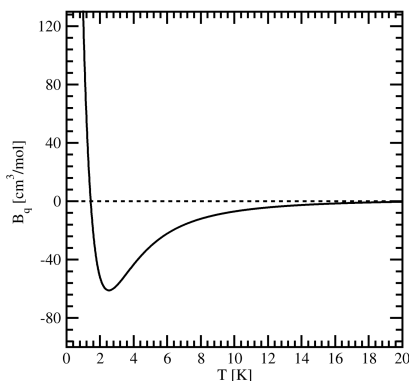
Fig. 2. The dependence of the quantum second virial coefficient B_q [cm^3/mol] on the temperature T [K] (for $T = 1$–20 K).

</div>
<div>

TABLE II

The classical second virial coefficient B_{cl} [cm^3/mol] and its first quantum correction B_{qc} [cm^3/mol], at different low temperatures T [K].

T [K]	B_{cl} [cm^3/mol]	B_{qc} [cm^3/mol]
20	-8.476×10^4	1.095×10^4
25	-2.222×10^4	1.747×10^3
30	-9.307×10^3	4.869×10^2
35	-5.046×10^3	1.880×10^2
40	-3.195×10^3	89.48
45	-2.234×10^3	49.11
50	-1.671×10^3	29.85
60	-1.066×10^3	13.61
70	-7.578×10^2	7.486
80	-5.760×10^2	4.652
90	-4.576×10^2	3.148
100	-3.751×10^2	2.267

more negative. It reaches a minimum, which represents the equilibrium point, at $T = 2.54$ K. The minimum value of B_q is $B_{min} = -61.11$ cm^3/mol. For $T > 2.5$ K, B_q becomes less negative with increasing T and it approaches zero in the higher limit of this T-range.

As neither experimental nor theoretical results are available in this T-range (5 mK–20 K), it is not possible to assess the accuracy of our results. However, the present framework has been successfully applied to a host of inert and other gases [11–13, 34, 35].

3.2. Classical second virial coefficient B_{cl} with first quantum correction B_{qc}

These have been calculated for the T-range (20–100 K), using (6) and (7). The results are presented in Table II. One can see that B_{cl} is negative over this entire range due to the presence of long-range attractive forces [39]. The contribution of short-range repulsive forces increases as T increases, causing B to become less negative. It is clear that B_{qc} is strongly temperature-dependent at low T. The results indicate that B_{qc} rapidly increases as T decreases. At $T \leq 60$ K, it is clear that B_{qc} plays a significant role and cannot be neglected. At $T > 60$ K, B_{qc} is negligible because the quantum effects are small.

The classical second virial coefficient B_{cl} can be fitted as a function of T. Its form is given as

$$B_{Fit} = a + bT + \frac{c}{T} + d \exp\left(-\frac{e}{T^2}\right), \quad (8)$$

where the fitting parameters in the regime of $T = 100$–10000 K are: $a = -829.241$ cm^3/mol, $b = -0.0015258$ cm^3/(mol K), $c = -13244.3$ cm^3 K/mol, $d = 870.593$ cm^3/mol and $e = 3789.03$ K^2.

Figure 3 shows B_{cl} and its fitting equation, B_{Fit}, in the T-range 100–10000 K. Clearly, the proposed fitting function accurately represents the behavior

</div>
</div>
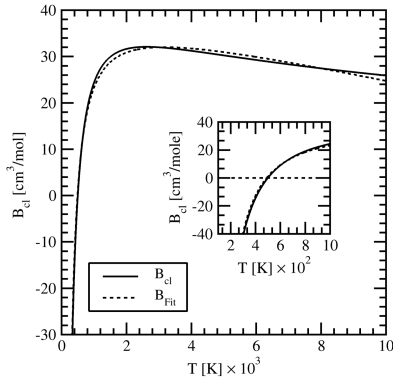
Fig. 3. The dependence of the classical second virial coefficient B_{cl} [cm^3/mol] and its fit B_{Fit}[cm^3/mol] on the temperature T [K] for high T (100–10000 K). The inset pertains to the lower T-range (100–1000 K).

of B_{cl} which is very negative at "low" T. By increasing T, B_{cl} becomes less negative and equals zero at the Boyle temperature ($T_B \approx 500.1$ K), where the attractive and repulsive forces are balanced. This result is in agreement with previous results [22, 40] of 507.22 K and 506 K, respectively. For $T > T_B$, B_{cl} becomes positive. It continues to increase with increasing T, until it passes through a maximum at a certain intermediate T, which is called the inversion temperature (T_i). The maximum $(B_{cl})_{max}$ occurs at $T_i \approx 2614$ K, which is associated with the Joule free expansion [41]. For $T > T_i$, B_{cl} decreases and decays towards zero at very high T.

The accuracy of the present results can be tested by comparing our B_{cl} and T_B to previous theoretical [17, 18, 22, 23] and experimental [25] results, as shown in Table III. It is found that the agreement is quite good. In each case, T_B is around 500 K. It is concluded that the Morse potential is quite successful in this context. For B_{cl}, the agreement is also good with Hellmann et al. [18], who used an intermolecular potential energy surface (PES) in their *ab initio* calculations, and with Somuncua et al. [17] who used the Kihara potential.

The average absolute relative deviation (AARD) for B_{cl} at different T has also been calculated for experimental data [25] as well as for theoretical calculations with the following potentials: (i) Morse (present); (ii) Kihara [17]; (iii) Lennard-Jones (LJ) of types 12-6 [22] and 21-6 [23]; and (iiii) PES [18]. The AARD is given by

$$\text{AARD} = \frac{1}{N} \sum_{i=1}^{N} \left| \left(\frac{B_{exp} - B_{cal}}{B_{exp}} \right)_i \right| \times 100, \quad (9)$$

where N, B_{cal} and B_{exp} are, respectively, the number of data, the calculated B and the experimental B. These AARD calculations are shown in Table IV. It is noted that the AARD for the present results is the lowest. This means that the present model surpasses the others.

3.3. Thermodynamic properties

Having obtained B, one can readily determine the pressure P, compressibility factor Z, internal energy U, the Helmholtz free energy F, entropy S and specific heat capacity C_v as follows [1, 42, 43]:

$$\frac{P}{nk_BT} = 1 + nB, \quad (10)$$

$$Z = 1 + nB, \quad (11)$$

$$U(T) \approx N \left[\frac{3}{2} k_B T - n k_B T^2 \frac{dB(T)}{dT} \right], \quad (12)$$

$$F = N k_B T \left[\ln(n\lambda^3) - 1 + nB(T) \right], \quad (13)$$

$$S = -\left(\frac{\partial F}{\partial T} \right)_V, \quad (14)$$

$$C_v = \left(\frac{dU}{dT} \right)_V. \quad (15)$$

The results have been calculated for the number density $n = 1 \times 10^{-4}$ Å^{-3} and the T-range 1–20 K, using B_q. These results are displayed in Figs. 4 and 5.
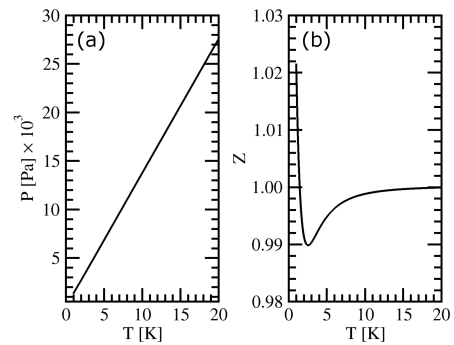
Fig. 4. (a) The pressure P [Pa] as a function of the temperature T [K]. (b) The compressibility factor Z as a function of T [K].
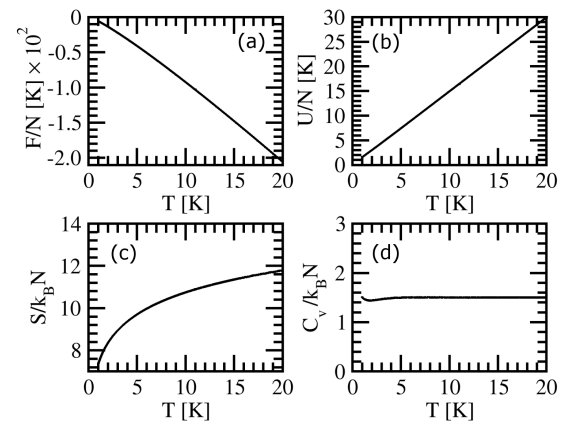
Fig. 5. Further thermodynamic properties of CH$_4$ as a function of the temperature T [K]: (a) the Helmholtz free energy per molecule, F/N [K], (b) the internal energy per molecule, U/N [K], (c) the entropy per molecule, S/k_BN, (d) the specific heat capacity C_v/k_BN.

TABLE III

Comparison of our results for the classical second virial coefficient B_{cl} [cm^3/mol] with previous results.

T [K]	B_{cl} [cm^3/mol]					
	Present results	Theor. [17]	Theor. [18]	Theor. [22]	Theor. [23]	Exp. [25]
105	−342.7	–	−369.32	–	–	–
110	−314.6	–	−336.59	–	−334.0	–
120	−268.4	–	−283.90	–	−281.1	–
130	−232.2	–	−243.44	–	−240.7	–
140	−203.0	–	−211.46	–	−208.8	–
160	−159.0	–	−164.25	–	−161.9	–
180	−127.5	–	−131.16	–	−129.2	–
200	−104.0	-105.905	−106.74	–	−105.1	–
250	−65.00	–	−66.94	–	−65.8	–
273.15	−52.75	–	−54.56	–	−53.6	–
293.15	−44.03	–	−45.79	−45.25	–	−44.95
298.15	−42.08	–	−43.82	–	–	–
300	−41.37	−42.0094	−43.11	–	−42.3	–
400	−14.51	−15.4109	−16.19	−15.75	−15.7	−15.09
450	−6.256	–	−7.92	–	−7.4	–
490	−1.079	–	−2.72	–	–	–
500	6.167×10^{-2}	-1.01061	−1.57	−0.82	−1.1	0.39
510	1.149	–	0.48	–	–	–
550	5.027	–	3.43	–	4.0	–
600	9.010	7.92903	7.47	8.55	8.1	10.43
650	12.26	–	10.78	–	11.5	–
700	14.95	13.967	13.53	14.91	14.3	17.51
800	19.11	18.2851	17.83	19.46	18.8	22.77
900	22.12	21.5034	21.00	22.84	22.1	26.83
1000	24.37	23.978	23.41	25.42	24.7	30.07
1200	27.42	–	26.75	29.06	29.8	34.92
1400	29.28	–	–	31.44	–	38.37
1600	30.44	–	–	33.05	–	40.95
1800	31.18	–	–	34.19	–	42.96
2000	31.64	–	–	35.00	–	44.56
2400	32.04	–	–	36.02	–	46.97

TABLE IV

Comparison of the average absolute relative deviation (AARD) in the calculation of B_{cl}, using (i) the Morse potential (present results), (ii) Kihara [17], (iii) Lennard-Jones (LJ) of types (12-6 [22] and 21-6 [23]) and (iiii) intermolecular potential energy surface (PES) [18].

	B_{cl} [cm^3/mol]				
	Present results	Theor. [17]	Theor. [18]	Theor. [22]	Theor. [23]
N	14	7	9	14	8
T-range [K]	293.15–2400	100–1000	293.15–1200	293.15–2400	293.15–1200
AARD	23.77%	66.47%	72.42%	36.60%	62.01%

The P–T curve is shown in Fig. 4a. It is observed that P rises monotonically with increasing T, and it is almost linear in this region of T. Figure 4b displays the Z–T curve. At very low T (≤ 5 K), Z is strongly-dependent on T; "nonideality" occurs. Further, Z decreases rapidly with increasing T and it reaches a minimum at about $T \approx 2.54$ K. For $T > 5$ K, Z decreases less rapidly and approaches 1 at $T = 15$–20 K. The same occurs at $T_B \approx 1.45$ K, with $B_q \to 0$. There, the system behaves as an ideal gas. Generally, the behavior of Z as a function of T is rather the same as the behavior of B_q.

Figure 5a displays F as a function of T. One can observe that F decreases linearly with increasing T. In contrast, U (see Fig. 5b) increases as T increases (with the kinetic energy increasing) and exhibits a linear dependence on T. Figure 5c indicates a substantive increase of S as T increases. Finally, C_v is plotted as a function of T in Fig. 5d. It is nearly independent of T, since $\frac{C_v}{Nk_\mathrm{B}} \approx 1.5$.

4. Conclusion

The subject of this work was the second virial coefficient B of CH_4 vapor in the broad temperature range (5 mK–10000 K). Specifically, B was computed in two temperature regions:

1. Temperature region $T = 5$ mK–20 K: the quantum second virial coefficient B_q was calculated. This is the first time that B_q for CH_4 has been studied. It was found that B_q behaves with T in much the same way as the behavior of the intermolecular CH_4–CH_4 potential with the intermolecular separation r;

2. Temperature region $T = 20$–10000 K: the classical second virial coefficient B_cl, the Boyle temperature T_B and the inversion temperature T_i were determined. Therefore, it was the first quantum correction B_qc for the T-region (20–100 K). It was found that it is necessary to make quantum corrections to the B_cl for $T = 20$–60 K, whereas the quantum effects for $T > 60$ K are relatively insignificant. In general, our results for B_cl are in good agreement with previous theoretical and experimental results.

Then, B_q was used to investigate the (pressure P–number density n–T) behavior of CH_4 vapor, as well as its other thermodynamic properties: the Helmholtz free energy F, internal energy U, entropy S, compressibility factor Z and specific heat capacity C_v in the T-region (1–20 K) for $n = 1 \times 10^{-4}$ Å^{-3}.

Acknowledgments

References

[1] S.M. Mosameh, A.S. Sandouqa, H.B. Ghassib, B.R. Joudeh, *J. Low Temp. Phys.* **175**, 523 (2014).

[2] J. Van Rijssel, V.F.D. Peters, J.D. Meeldijk, R.J. Kortschot, R.J.A. van Dijk-Moes, A.V. Petukhov, B.H. Erné, A.P. Philips, *J. Phys. Chem. B* **118**, 11000 (2014).

[3] G.A. Vliegenthart, H.N.W. Lekkerkerker, *J. Chem. Phys.* **112**, 5364 (2000).

[4] G.E. Uhlenbeck, E. Beth, *Physica* **3**, 729 (1936).

[5] E. Beth, G.E. Uhlenbeck, *Physica* **4**, 915 (1937).

[6] V.L. Seguin, H. Guignes, C. Lhuillier, *Phys. Rev. B* **36**, 141 (1987).

[7] H.B. Ghassib, R.F. Bishop, M.R. Strayer, *J. Low Temp. Phys.* **23**, 393 (1976).

[8] E.V.L. Mello, J.J. Rehr, O.E. Vilches, *Phys. Rev. B* **28**, 3759 (1983).

[9] R.T. Pack, *J. Chem. Phys.* **78**, 7217 (1983).

[10] H.B. Ghassib, A.S. Sandouqa, B.R. Joudeh, S.M. Mosameh, *Can. J. Phys.* **92**, 997 (2014).

[11] O.T. Al-Obeidat, A.S. Sandouqa, B.R. Joudeh, H.B. Ghassib, M.M. Hawamdeh, *Can. J. Phys.* **95**, 1208 (2017).

[12] A.S. Sandouqa, B.R. Joudeh, O.T. Al-Obeidat, M.M. Hawamdeh, H.B. Ghassib, *Eur. Phys. J. Plus* **135**, 161 (2020).

[13] A.S. Sandouqa, *Chem. Phys. Lett.* **703**, 29 (2018).

[14] J.J. Novoa, M.H. Whangbo, *J. Chem. Phys.* **94**, 4835 (1991).

[15] O. Akin-Ojo, A.H. Harvey, K. Szalewicz, *J. Chem. Phys.* **125**, 014314 (2006).

[16] A. Skorek, R. Włodarczyk, *J. Ecol. Eng.* **19**, 172 (2018).

[17] E. Somuncua, M. Emek, B.A. Mamedov, *Acta Phys. Pol. A* **137**, 293 (2020).

[18] R. Hellmann, E. Bich, E. Vogel, *J. Chem. Phys.* **128**, 214303 (2008).

[19] R. Hellmann, E. Bich, V. Vesovic, *J. Chem. Phys.* **144**, 134301 (2016).

[20] H. Peyrovedin, F. Essmaeizadeh, M. Binzadeh, *Fluid Phase Equilib.* **492**, 88 (2019).

[21] U. Hohm, K. Kerl, *Ber. Bunsen-Ges.* **95**, 36 (1991).

[22] A. Hutem, S. Boonchui, *J. Math. Chem.* **50**, 1262 (2012).

[23] J.M.H. Levelt-Sengers, M. Klein, J.S. Gallagher, Report AEDC-TR-71-39, Arnold Engineering and Development Centre, Tullahoma (TN) 1971.

[24] A. Boushehri, J. Bzowski, J. Kestin, E.A. Mason, *J. Phys. Chem. Ref. Data* **16**, 445 (1987).

[25] J.H. Dymond, E.B. Smith, *The Virial Coefficients of Pure Gases and Mixtures. A Critical Compilation*, Clarendon, Oxford 1980.

[26] M.A. Byrne, M.R. Jones, L.A.K. Staveley, *Trans. Faraday Soc.* **64**, 1747 (1968).

[27] D.R. Douslin, R.H. Harrison, R.T. Moore, J.P. MuCullough, *J. Chem. Eng. Data* **9**, 358 (1964).

[28] W. Wagner, K.M. de Reuck, *Methane. International Thermodynamic Tables of the Fluid State-13, International Union of Pure and Applied Chemistry*, Blackwell, Oxford 1996.

[29] Y. Song, L. Marrodán, N. Vin et al., *Proc. Combust. Inst.* **37**, 667 (2019).

[30] B.A. Mamedov, E. Somuncu, *Physica A* **420**, 246 (2015).

[31] R.J. Sadus, *J. Chem. Phys.* **150**, 024503 (2019).

[32] A.N. Akour, A.S. Sandouqa, B.R. Joudeh, H.B. Ghassib, *Chin. J. Phys.* **56**, 411 (2018).

[33] A.F. Al-Maaitah, A.S. Sandouqa, B.R. Joudeh, H.B. Ghassib, *Int. J. Mod. Phys. B* **31**, 1750202 (2017).

[34] A.F. Al-Maaitah, A.S. Sandouqa, B.R. Joudeh, O.T. Al-Obeidat, *Chin. J. Phys.* **62**, 194 (2019).

[35] O.T. Al-Obeidat, A.S. Sandouqa, B.R. Joudeh, M.M. Hawamdeh, H.B. Ghassib, *Phys. Scr.* **95**, 015401 (2020).

[36] J.M. Blatt, *Nuovo Cim.* **4**, 430 (1956).

[37] B.P. Reid, M.J. O'Loughlin, R.K. Sparks, *J. Chem. Phys.* **83**, 5656 (1985).

[38] A. Matsumoto, *Z. Nat.forsch.* **42a**, 447 (1987).

[39] A.S. Sandouqa, B.R. Joudeh, *Phys. Scr.* **93**, 095401 (2018).

[40] J.A. Beattie, W.H. Stockmayer, *J. Chem. Phys.* **10**, 473 (1942).

[41] E. Albarrán-Zavala, B. Kok, A. Espinoza-Elizarrarazubo, F. Angulo-Brown, *Open Thermodyn. J.* **3**, 17 (2009).

[42] R.P. Feynman, *Statistical Mechanics*, Benjamin, Reading (MA) 1992.

[43] B.A. Mamedov, E. Somuncu, *Chin. J. Phys.* **55**, 1473 (2017).